基于响应面法的低碳贝氏体钢激光-电弧复合焊接工艺参数优化

余杰，蔡创*，谢佳，梁盈，黄嘉森，刘致杰，刘永洪

西南交通大学材料科学与工程学院材料先进技术教育部重点实验室，四川 成都 610031

摘要　选用 6 mm 厚低碳贝氏体钢板进行激光-MAG 复合焊接（MAG 焊，熔化极活性气体保护电弧焊），以激光功率、焊接速度、送丝速度为试验参数，以焊缝成形系数（ψ）、激光区面积比（R）为响应指标，建立响应面分析数学模型。送丝速度对 ψ 和 R 的影响显著，激光功率与焊接速度的交互作用对 ψ 的影响显著，送丝速度与焊接速度的交互作用对 R 的影响显著。对焊缝成形进行评定，筛选出最优工艺参数：激光功率 4120～4300 W，焊接速度 15.3～16.3 mm/s，送丝速度 12.3～13.6 m/min。经试验验证，ψ 和 R 的模型准确度分别为 95.0% 和 92.3%。

关键词　激光技术；激光-MAG 复合焊接；低碳贝氏体钢；响应面法；成形系数；激光区面积比

中图分类号　TG457.1　　　**文献标志码**　A　　　　　　　　　　**DOI**：10.3788/CJL202249.1602018

1　引　言

低碳贝氏体钢因具有韧性强、比强度大等优点，已成为高速列车转向架的主要制造材料[1]。转向架中存在诸多对接接头和 T 型接头，迫切需要高效率和高质量的焊接技术。激光焊具有能量密度高、焊接热影响区窄、熔深大的特点，但其装配要求严格、耗时长；电弧焊具有坡口适应性强的特点，但热源能量密度低、焊接速度小、残余应力较大[2-6]。随着转向架制造要求的不断提高，单一热源焊接技术在制造过程中暴露出诸多问题，复合焊接技术得到了广泛关注。激光-电弧复合焊接可改善单激光焊接中装配要求严格、耗时长的问题，同时还具有弧焊坡口适应性强的优点，可大幅提高焊接效率，减少焊接缺陷，改善焊缝形貌[7-10]。焊缝形貌优劣是评价焊接质量好坏的最直观指标[11]。在激光-电弧复合焊中，激光功率、焊接速度、送丝速度等关键焊接参数的变化以及各焊接参数之间的交互作用均会影响焊缝成形，因此复合焊工艺参数优化的成本高、耗时长[12-15]。借助响应面法（RSM）研究各参数及参数间交互作用对响应指标的影响有利于实现激光-电弧复合焊接工艺参数的优化。

在 RSM 法中，通过建立焊接工艺参数与响应指标的数学模型，表征各工艺参数及其相互作用对响应指标的影响，并将响应指标的变化通过三维响应曲面图或等高线呈现[16-17]。在焊接领域中，响应面法主要被应用于激光焊、搅拌摩擦焊、电弧焊和埋弧焊等焊接技术中，可表征各焊接参数对气孔率和焊接接头形貌的影响[18-21]。Ragavendran 等[22]将响应面法运用于奥氏体不锈钢的脉冲激光-TIG 焊接参数优化中（TIG 焊，非熔化极惰性气体保护电弧焊），二次回归模型显示，电流、焊速、电弧间隙、焊头角度与偏振度（DOP）的相互作用对响应指标的影响显著。Reisgen 等[23]基于响应面法设计，建立了关于双相 DP600/TRIP700 钢激光焊接工艺参数的数学模型，优化了工艺参数，提高了焊接质量和生产率，并降低了成本。Wang 等[24]使用响应面法建立了激光功率、连接速度、夹紧压力、扫描次数、连接强度、连接宽度与连接成本之间的数学模型，并筛选出最优工艺参数。Benyounis 等[25-26]将响应面法用于激光焊焊缝几何形状预测，分析了焊接工艺参数对焊缝形貌的影响。综上所述，大多数研究侧重于将响应面法应用于单一热源焊接工艺优化，关于复合热源响应面优化分析的研究较少。

本文对 6 mm 厚低碳贝氏体钢对接接头进行了激光-MAG 复合焊（MAG 焊，熔化极活性气体保护电弧焊），分析并评估了激光功率、焊接速度和送丝速度对焊缝成形的影响，确定试验参数水平。通过 Box-behnken 设计试验，选取激光功率、焊接速度和送丝速度为试验因素，选取焊缝成形系数和激光区面积比为响应指标。基于响应面法，建立了关于激光功率、焊接速度、送丝速度与响应指标的数学模型，探索了各参数

及参数间交互作用对焊缝形貌的影响规律,筛选出焊接工艺优化区间,并进行了试验验证。研究结果为高速列车转向架用新型低碳贝氏体钢的激光-MAG 复合焊工艺的开发提供了技术参考。

2 试验材料与方法

2.1 试验材料

采用尺寸为 350 mm×175 mm×6 mm 的新型低碳贝氏体钢板,所用焊丝为直径为 1.2 mm、强度为 800 MPa 量级的低合金高强钢焊丝,两者成分如表 1 所示。

2.2 试验方法

所用光纤激光器的最大激光功率为 10 kW,激光波长为 1070 nm,焦距为 350 mm。电弧焊接系统为 Fronius TransPuls Synergic 4000 型焊机,激光-电弧复合焊接系统还包含机器人和集成操作控制柜。激光-MAG 复合焊采用激光引导模式,图 1 所示为激光-MAG 复合焊接示意图及坡口示意图,采用 I 型坡口,

对接间隙为 1 mm,实现单面焊双面成形。焊接试板放置在水平工作台上,为防止焊接过程中激光反射损坏激光器内部结构,设置激光束与竖直方向夹角为 10°,焊枪与试板的夹角为 40°。在焊接过程中,激光离焦量为 0 mm,光丝间距为 2 mm,保护气为体积比为 4∶1 的 Ar、CO_2 混合气体,流量为 25 L/min。

利用蔡司显微镜观察并拍摄焊接接头形貌,采用 Image-Pro 软件对不同工艺参数下焊接接头的熔宽（W）、熔深（H）、电弧区面积（S_1）和激光区面积（S_2）进行测量,并计算得到焊缝成形系数（ψ）和激光区面积比（R）。ψ 和 R 分别表征焊缝形状尺寸与激光电弧能量中激光能量占比:

$$\psi = \frac{W}{H}, \quad (1)$$

$$R = \frac{S_2}{S_1 + S_2}。 \quad (2)$$

焊缝测量区域示意图如图 2 所示。

表 1 低碳贝氏体钢和焊丝主要化学成分（质量分数,％）

Table 1 Chemical compositions of low-carbon bainite steel and welding wire (mass fraction,％)

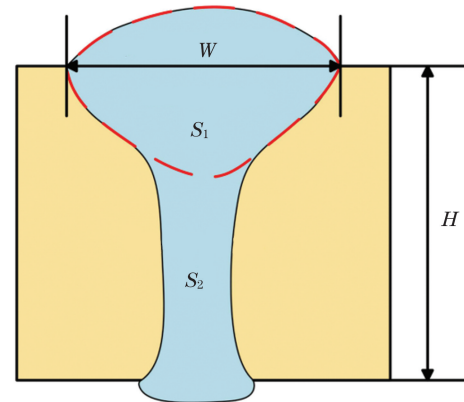| Element	C	Si	Mn	Cr	Ni	Mo	Cu	Nb	Ti	Co	Fe
Low-carbon bainite steel	0.04	0.3	1.35	0.33	0.53	0.34	0.35	0.03	0.02	<0.01	Bal.
Welding wire	0.06	0.37	1.49	0.34	2.84	0.35	0.1	—	—	—	Bal.
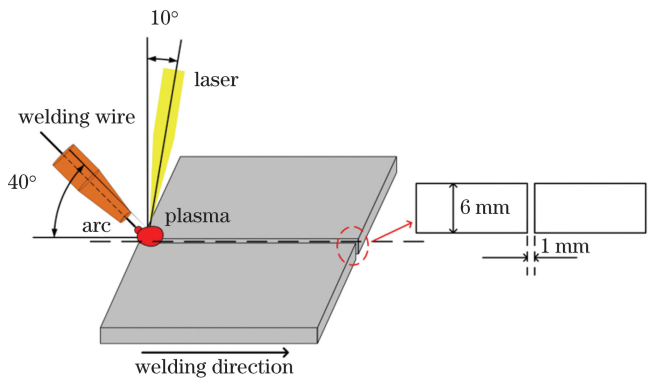
图 1 激光-电弧复合焊接系统和坡口示意图

Fig. 1 Schematics of laser-arc hybrid welding system and groove

图 2 焊缝测量区域示意图

Fig. 2 Schematic of weld measurement area

2.3 因素水平确定

对 6 mm 厚的低碳贝氏体钢进行激光-MAG 复合焊,分别设置焊接速度（V_w）和送丝速度（V_f）为 18 mm/s 和 13 m/min,激光功率（P）设置为 3000,3500,4000,4500,5000 W。其中 P 为 3000 W 和 3500 W 时均未焊透,P 为 5000 W 时焊缝塌陷,故激光功率控制在 4000～4500 W 范围内。分别设置激光功率和焊接速度为 4000 W 和 18 mm/s,送丝速度设置为 9～14 m/min,其中 V_f＝9～12 m/min 时未焊透,故送丝速度控制在 12～14 m/min 范围内。分别设置激光功率和送丝速度为 4000 W 和 13 m/min,焊接速度设置为 12～27 mm/s,当 V_w＝12～14 mm/s 时,焊缝背面出现焊瘤,当 V_w＞18 mm/s 时未焊透,

故焊接速度控制在 14～18 mm/s 范围内。利用 Design-Expert 软件对焊接参数进行编码转换,得到工艺参数因素水平表,如表 2 所示。

表 2 低碳贝氏体钢激光-MAG 复合焊接的工艺参数水平

Table 2 Process parameter levels for laser-MAG hybrid welding of low-carbon bainite steel

Experimental factor	Value		
	Low level	Zero level	High level
P/W	4000	4250	4500
V_w/(mm·s^{-1})	14	16	18
V_f/(m·min^{-1})	12	13	14

2.4 建立回归模型

本文将焊缝成形系数 ψ 和激光区面积比 R 作为

响应指标,使用 Design-Expert 软件对三因素 P、V_f、V_w 以及响应指标 ψ、R 进行二次多项式拟合。二次多项式方程[27]可表示为

$$y = b_0 + \sum_{j=1}^{p} b_j x_j + \sum_{i<j}^{p} b_{ij} x_i x_j + \sum_{j=1}^{p} b_{jj} x_j^2,$$

$$(3)$$

式中:y 为试验响应;x 为试验因素;b_0 为方程常数项;b_j 为一次项系数;b_{ij} 为交叉项系数;b_{jj} 为二次项系数;i 和 j 为试验因素编号;p 为试验因素个数。模型公式主要由常数项、一次项、交叉项及平方项组成,一次项为影响试验因素的主效应,交叉项与平方项为交互效应。通过方差分析对所建立模型中的每一项进行回归显著性检验,获得模型显著项及显著水平。依据试验结果,在 Design-Expert 软件上拟合等高线图和响应面曲面图,分析响应值的优化范围,获得优化参数区间。

3 结果与分析

3.1 焊缝横截面宏观形貌与成形试验结果

结合表 2 的因素水平,运用 Design-Expert 响应面试验设计模块设计试验矩阵表,并按照随机方式排列试验顺序,以避免系统误差。分别计算并统计焊缝成形系数 ψ 和激光区面积比 R,统计结果如表 3 所示。部分焊接接头成形与横截面形貌如表 4 所示。

3.2 回归模型

根据试验因素及响应值统计结果,建立的焊缝成形系数数学模型为

$$\psi = 10.64 + 7.25A - 1.21B - 2.28C + 0.11AB + 0.15AC + 0.01BC - 1.29A^2 + 0.01B^2 + 0.06C^2,$$

$$(4)$$

式中:A、B、C 分别表示模型中激光功率、焊接速度和送丝速度这三个因素。

其方差分析结果如表 5 所示,其中 F 值为 F 分布检验统计值,P 值为模型可靠性统计检验值,R^2 为模型拟合度,R_{adj}^2 为修正拟合系数。由 F 检验可知:F 值的计算结果为 8.80,模型显著。通过 P 值筛选出成形系数模型的显著项为 B、C 和 AB 项;该模型 R^2 及 R_{adj}^2 分别为 0.919 和 0.814,信噪比(模型方差与残差的比值)为 11.15,大于 4。以上模型检验均表明,利用所测量数据进行回归建模是可行的,能获得较准确的焊缝成形系数数学模型。

表 3 低碳贝氏体钢激光-MAG 复合焊的试验参数和响应值统计

Table 3 Statistics of test parameters and response values for laser-MAG hybrid welding of low-carbon bainite steel

Process No.	Laser power P/W	Welding speed V_w/(mm·s⁻¹)	Wire feeding speed V_f/(m·min⁻¹)	Weld forming coefficient ψ	Laser area ratio R
1	4000	16.00	14.00	1.124	0.2355
2	4250	16.00	13.00	1.278	0.2589
3	4250	14.00	12.00	1.470	0.2119
4	4000	14.00	13.00	1.406	0.3054
5	4000	16.00	12.00	1.009	0.1634
6	4250	16.00	13.00	1.116	0.2280
7	4500	16.00	14.00	1.283	0.2806
8	4250	18.00	12.00	0.874	0.2196
9	4250	14.00	14.00	1.574	0.6008
10	4000	18.00	13.00	0.884	0.1103
11	4250	16.00	13.00	1.089	0.2093
12	4500	16.00	12.00	1.014	0.1830
13	4250	16.00	13.00	1.064	0.1899
14	4500	18.00	13.00	0.919	0.1310
15	4250	16.00	13.00	1.100	0.2199
16	4500	14.00	13.00	1.216	0.2562
17	4250	18.00	14.00	1.068	0.1928

表 4　低碳贝氏体钢激光-MAG 复合焊接头成形和横截面形貌

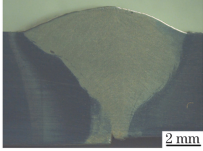Table 4　Weld formation and cross-sectional morphology of low-carbon bainitic steel joint by laser-MAG hybrid welding
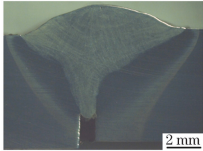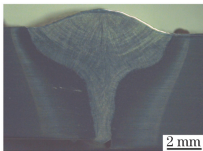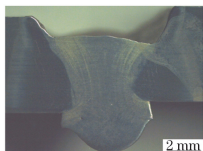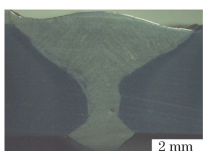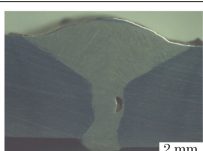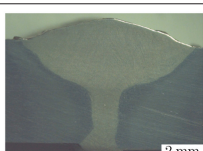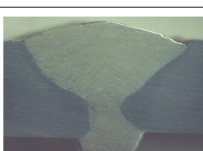
Process No.	Front appearance of weld surface	Cross-sectional morphology	Weld formation
2	2# 20 mm	2 mm	Excess weld accumulation
5	5# 20 mm	2 mm	Lack of penetration
6	6# 20 mm	2 mm	Good form
9	9# 20 mm	2 mm	Excessive penetration and overlap
13	13# 20 mm	2 mm	Undercut
15	15# 20 mm	2 mm	Pores
16	16# 20mm	2 mm	Good form
17	17# 20 mm	2 mm	Undercut

表 5　焊缝成形系数模型的方差分析

Table 5　Variance analysis of models for weld forming coefficient model

Source	Sum of squares	Degree of freedom	Mean square	F value	P value	Reliability
Model	0.59	9	0.066	8.80	0.0045	Significant
A	1.075×10^{-5}	1	1.075×10^{-5}	1.434×10^{-3}	0.9709	
B	0.46	1	0.46	61.44	0.0001	
C	0.058	1	0.058	7.76	0.0271	
AB	0.013	1	0.013	1.70	0.0958	
AC	5.863×10^{-3}	1	5.863×10^{-3}	0.78	0.4060	
BC	2.015×10^{-3}	1	2.015×10^{-3}	0.27	0.6203	

续表

Source	Sum of squares	Degree of freedom	Mean square	F value	P value	Reliability
A^2	0.028	1	0.028	3.70	0.2335	
B^2	0.014	1	0.014	1.89	0.2118	
C^2	0.015	1	0.015	1.96	0.2041	
Residual	0.053	7	7.502×10^{-3}			
Lack of fitting value	0.023	3	7.818×10^{-3}	1.08	0.4538	Not significant
Pure error	0.029	4	7.266×10^{-3}			
Total	0.65	16	0.066			

利用所测量数据,建立了激光区面积比回归模型:

$$R = -6.015 + 6.174A - 0.157B - 0.869C + 0.035AB + 0.025AC - 0.023BC - 0.829A^2 + 0.008B^2 + 0.046C^2 \text{。} \tag{5}$$

表 6 为激光区面积比模型的方差分析结果。由 F 检验可知:F 值的计算结果为 6.61,模型显著;在本模型中,B、C 和 BC 为模型的显著项;该模型 R^2 及 R_{adj}^2 分别 0.895 和 0.759,信噪比为 11.06,大于 4。以上检验结果表明,利用所测量数据建立的激光区面积比回归模型的可信度良好。

表 6 激光区面积比模型的方差分析

Table 6 Variance analysis of models for laser area ratio model

Source	Sum of squares	Degree of freedom	Mean square	F value	P value	Reliability
Model	0.19	9	0.021	6.61	0.0105	Significant
A	1.638×10^{-4}	1	1.638×10^{-4}	0.052	0.8254	
B	0.11	1	0.11	36.15	0.0005	
C	0.039	1	0.039	12.63	0.0093	
AB	1.222×10^{-3}	1	1.222×10^{-3}	0.39	0.5516	
AC	1.626×10^{-4}	1	1.626×10^{-4}	0.052	0.8261	
BC	8.621×10^{-3}	1	8.621×10^{-3}	2.76	0.0989	
A^2	0.011	1	0.011	3.62	0.1407	
B^2	4.135×10^{-3}	1	4.135×10^{-3}	1.32	0.2878	
C^2	9.002×10^{-3}	1	9.002×10^{-3}	2.88	0.1334	
Residual	0.022	7	3.125×10^{-3}			
Lack of fitting value	0.019	3	6.427×10^{-3}	9.92	0.0252	Not significant
Pure error	2.591×10^{-3}	4	6.476×10^{-4}			
Total	0.21	16				

3.3 焊缝成形系数响应面分析

图 3(a)为焊缝成形系数的散点分布图,试验值接近预测值,表明成形系数数学模型的预测能力较好。图 3(b)所示的单因素扰动曲线表明,随着激光功率 P 的增大,ψ 先增加后降低;随着焊接速度 V_w 的增大,ψ 逐渐降低;随着送丝速度 V_f 的增大,ψ 缓慢增大。当 $P < 4250$ W 时,激光功率增大,热源能量增加,导致熔深和熔宽增加,ψ 增大;当 $P > 4250$ W 时,由于能量过大,熔化金属增多,背部无法承受熔池重力,熔融金属向下流动,焊缝背面熔透较多,表面塌陷,出现表 4 中第 9、17 组工艺参数下的成形形貌。随着 V_w 的增加,热源作用时间减少,焊接热量降低,焊缝熔深和熔宽相应减小,ψ 减小。随着 V_f 的增加,电弧电流增加,电弧等离子体增多,电弧等离子体对光致等离子体的稀释作用增强,激光利用率增大,熔宽和熔深均增大,ψ 增大。

P 和 V_w 与成形系数 ψ 的交互作用如图 3(c)、(d)所示,其中颜色越深,表示因素影响越显著。响应曲面图在小激光功率、低焊接速度处的颜色较深,ψ 较大,即 $P = 4000 \sim 4300$ W,$V_w = 14 \sim 15$ mm/s 时,激光作用时间长,熔化金属体积大,故焊缝熔深和熔宽较大。依据实际成形较好时的第 6、16 组工艺参数,确定 $\psi = 1.1 \sim 1.2$,对应最优参数区间为 $P = 4000 \sim 4300$ W 和 $V_w = 15.1 \sim 16.3$ mm/s。P 和 V_f 与成形系数 ψ 的交互作用如图 3(e)、(f)所示。响应面为中间凸起的拱形图像,深色区域集中在 P 及 V_f 较大的区间,相较于 P,V_f 对 ψ 的影响更加显著。在较低激光功率下,ψ 维持在较低水平,当 $P = 4150 \sim 4550$ W 时,ψ 随 V_f 的增大而增大,当 $P > 4550$ W 时,V_f 对熔深的影响不显著。可以看出激光和电弧的相互作用存在一定限度,在合理的工艺范围内两者能有效地发挥耦合效应。结合实际成形状况,理想参数区间为 $P = 3970 \sim 4370$ W 和 $V_f = 10.9 \sim 14.5$ m/min。V_w 和 V_f 与成形系数 ψ
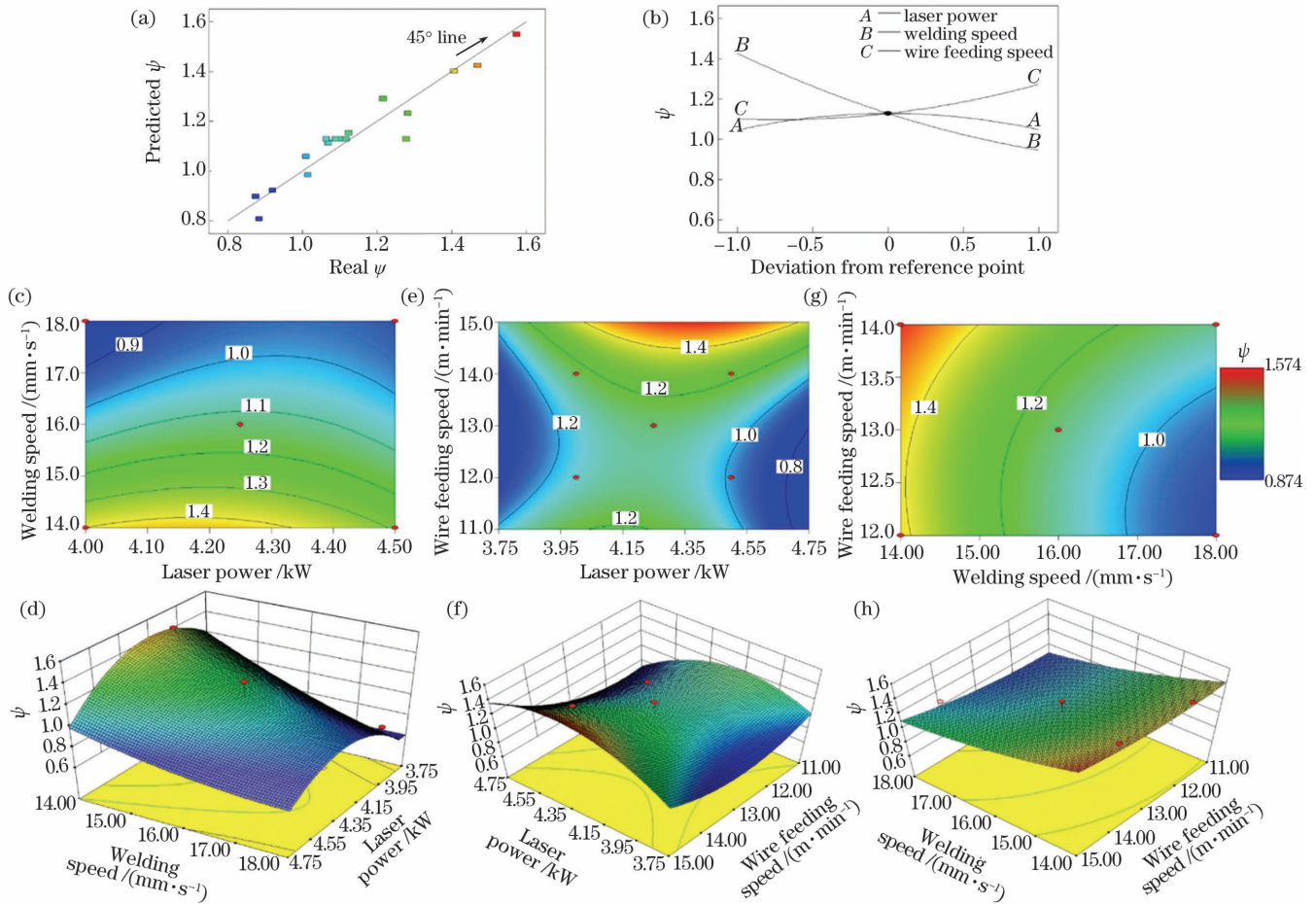
图 3 焊缝成形系数的影响曲线。(a)散点分布图；(b)单因素扰动曲线；(c)表征 P 和 V_w 与 ψ 的交互作用的等高线；(d)表征 P 和 V_w 与 ψ 的交互作用的响应面；(e)表征 P 和 V_f 与 ψ 的交互作用的等高线；(f)表征 P 和 V_f 与 ψ 的交互作用的响应面；(g)表征 V_w 和 V_f 与 ψ 的交互作用的等高线；(h)表征 V_w 和 V_f 与 ψ 的交互作用的响应面

Fig. 3 Influence curves of weld forming coefficient. (a) Scattered point distribution; (b) single factor disturbance curves; (c) contour lines characterizing interactions of P and V_w with ψ; (d) response surface characterizing interactions of P and V_w with ψ; (e) contour lines characterizing interactions of P and V_f with ψ; (f) response surface characterizing interactions of P and V_f with ψ; (g) contour lines characterizing interactions of V_w and V_f with ψ; (h) response surface characterizing interactions of V_w and V_f with ψ

的交互作用图如图 3(g)、(h)所示，深色区域主要集中在低焊接速度区，V_w 对成形系数 ψ 的影响较大，随着 V_w 的增大，熔深减小，ψ 减小；V_f 对成形系数 ψ 的影响相对较小，在较低焊接速度下，V_f 对熔深的影响不显著，在较高焊接速度下，V_f 对熔深的影响逐渐增大，结合实际成形状况，获得最优参数区间为 $V_w=15.3\sim16.6$ mm/s 和 $V_f=12.3\sim13.6$ m/min。

3.4 激光区面积比响应面分析

图 4(a)、(b)分别为各组试验参数下焊缝的激光区面积比 R 的散点分布图与单因素扰动曲线。试验值接近预测值，表明激光区面积比数学模型的预测能力较好。随着 P 的增大，R 先增大后减小。当 $P<4250$ W 时，热源能量随 P 的增大而增大，金属熔化较多，R 增大；当 $P>4250$ W 时，激光使电弧等离子体温度升高，逆韧致吸收效应增强，但菲涅耳吸收效应被削弱，R 减小。随着 V_w 的增大，热源作用时间减少，

匙孔深度相对减小，激光区面积减少，R 降低。随着 V_f 的增大，电弧电流增大，激光电弧耦合作用增强，R 呈逐渐上升的趋势。

P 和 V_w 与 R 的交互作用如图 4(c)、(d)所示，低焊接速度区间的 R 较大，主要是因为 V_w 较低，热源作用时间相对较长，热量较大，熔融金属较多。结合表 4 中第 6、16 组工艺参数可知，$R=0.2\sim0.3$ 时焊缝成形较好，对应的优化参数区间为 $P=4120\sim4300$ W 和 $V_w=14.8\sim16.4$ mm/s。P 和 V_f 与 R 的交互作用如图 4(e)、(f)所示，颜色较浅，两者对 R 的影响较小，均保持在低水平状态。当 $R=0.2\sim0.3$ 时，对应的最优参数区间为 $P=4100\sim4320$ W 和 $V_f=10.6\sim13.9$ m/min。V_w 和 V_f 与 R 的交互作用如图 4(g)、(h)所示，在较高焊接速度下，V_f 对 R 的影响较小。当 $R=0.2\sim0.3$ 时，理想参数区间为 $V_w=13.9\sim16.4$ mm/s 和 $V_f=11.5\sim13.6$ m/min。
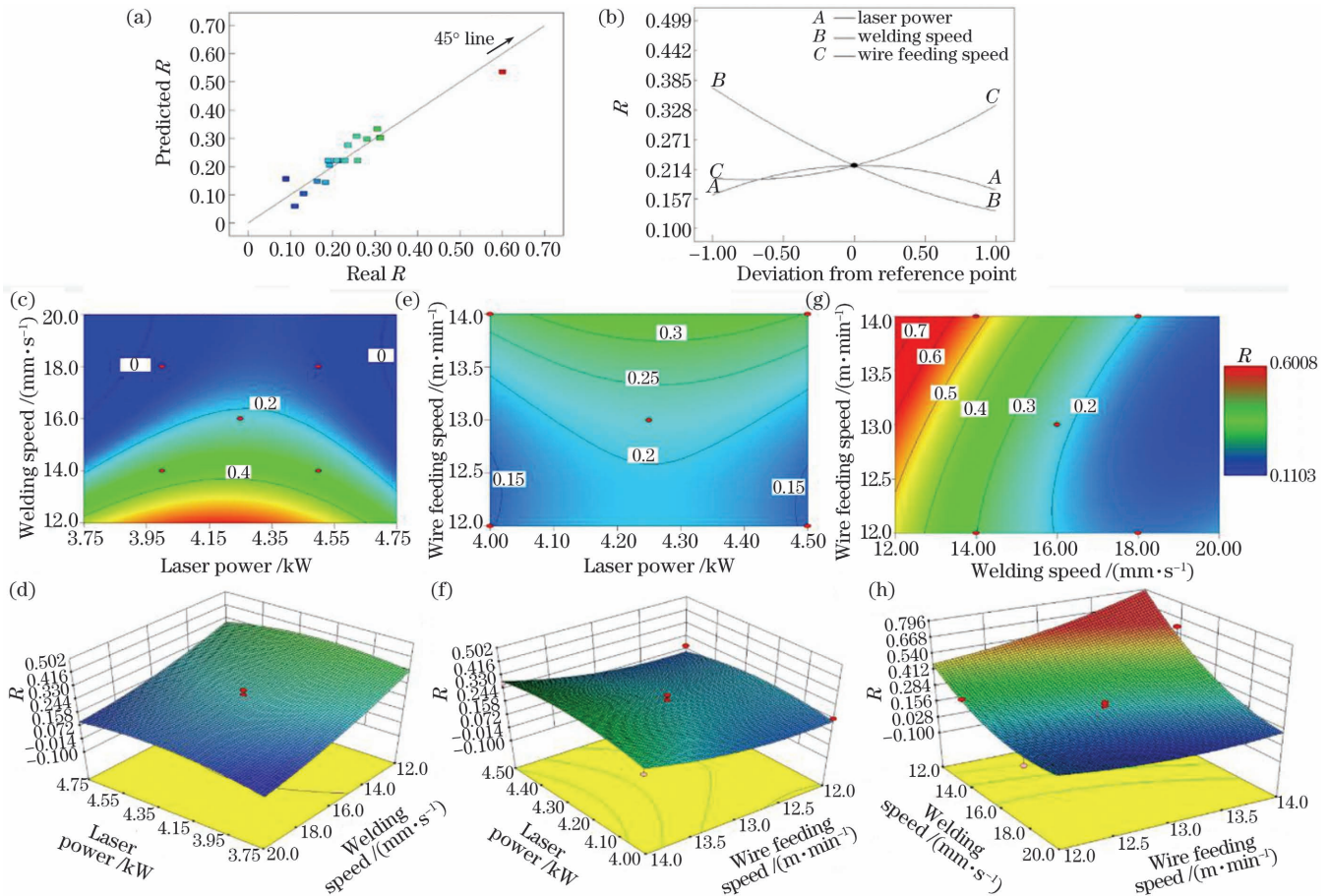
图 4 激光区面积比的影响曲线。(a)散点分布图;(b)单因素扰动曲线;(c)表征 P 和 V_w 与 R 的交互作用的等高线;(d)表征 P 和 V_w 与 R 的交互作用的响应面;(e)表征 P 和 V_f 与 R 的交互作用的等高线;(f)表征 P 和 V_f 与 R 的交互作用的响应面;(g)表征 V_w 和 V_f 与 R 的交互作用的等高线;(h)表征 V_w 和 V_f 与 R 的交互作用的响应面

Fig. 4 Influence curves of laser area ratio. (a) Scattered point distribution; (b) single factor disturbance curves; (c) contour lines characterizing interactions of P and V_w with R; (d) response surface characterizing interactions of P and V_w with R; (e) contour lines characterizing interactions of P and V_f with R; (f) response surface characterizing interactions of P and V_f with R; (g) contour lines characterizing interactions of V_w and V_f with R; (h) response surface characterizing interactions of V_w and V_f with R

3.5 焊接工艺参数的优化结果与试验验证

结合焊缝实际成形(第 6、16 组工艺参数下的焊缝成形良好),确定响应指标为 $\psi=1.1\sim1.2$,$R=0.2\sim0.3$,得到最终优化工艺参数区间为 $P=4120\sim4300$ W,$V_w=15.3\sim16.3$ mm/s,$V_f=12.3\sim13.6$ m/min,如表 7 所示。当 $P=4250$ W、$V_w=16$ mm/s,$V_f=13$ m/min 时,ψ 和 R 的模型预测值分别为 1.13 和 0.24。分别选择 $P=4250$ W、$V_w=$

16 mm/s,$V_f=13$ m/min 与 $P=4200$ W、$V_w=15.5$ mm/s,$V_f=13$ m/min 进行焊接试验验证。ψ 和 R 的试验统计结果如表 8 所示,可以看出,试验值与模型预测值接近。优化工艺参数下的典型焊缝形貌如图 5 所示,焊缝成形均匀,无咬边、焊瘤等宏观缺陷。对两次试验得到的 ψ 和 R 取平均值,分别为 1.19 和 0.26,利用预测值与平均值的比值得到 ψ 和 R 模型的准确度分别为 95.0% 和 92.3%。

表 7 低碳贝氏体钢激光-MAG 焊的优化工艺参数区间

Table 7 Optimized process parameter range for laser-MAG hybrid welding of low-carbon bainite steel

Response indicator	Laser power P /W	Welding speed V_w/(mm·s^{-1})	Wire feeding speed V_f/(m·min^{-1})
$\psi=1.1-1.2$	4000-4300	15.3-16.3	12.3-13.6
$R=0.2-0.3$	4120-4300	14.8-16.4	11.5-13.6
Optimal interval	4120-4300	15.3-16.3	12.3-13.6

表 8　ψ 和 R 的试验统计结果

Table 8　Statistical test results of ψ and R

Test parameter			ψ	R	Average value		Accuracy /%	
P /W	$V_{\mathrm{w}}/(\mathrm{mm\cdot s^{-1}})$	$V_{\mathrm{f}}/(\mathrm{m\cdot min^{-1}})$			ψ	R	ψ	R
4250	16.0	13	1.15	0.24	1.19	0.26	95.0	92.3
4200	15.5	13	1.23	0.27				
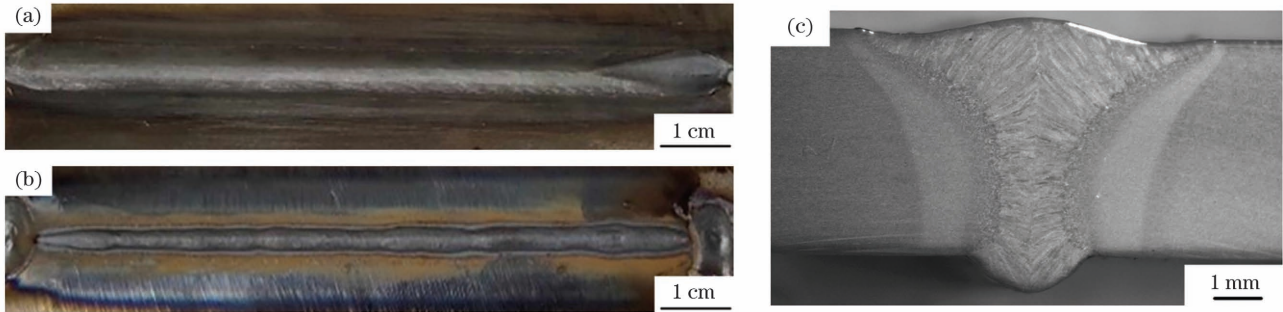
图 5　优化工艺参数（$P = 4250$ W，$V_{\mathrm{f}} = 16$ mm/s，$V_{\mathrm{f}} = 13$ m/min）下的典型焊缝形貌。(a)正面，(b)背面，(c)横截面

Fig. 5　Typical weld morphologies under optimized process parameters ($P = 4250$ W，$V_{\mathrm{w}} = 16$ mm/s, and $V_{\mathrm{f}} = 13$ m/min). (a) Front side; (b) back side; (c) cross-section

4　结　　论

利用 6 mm 厚高速列车转向架用低碳贝氏体钢进行激光-MAG 复合焊，建立响应面模型，优化焊接工艺参数，并进行试验验证，得到如下结论。

1）在不同激光功率、焊接速度、送丝速度下，基于响应面法建立了低碳贝氏体钢激光-MAG 复合焊接接头外观质量（焊缝成形系数和激光区面积比）的统计模型。

2）在响应面分析数学模型中，送丝速度对 ψ、R 的影响显著；焊接速度与 ψ、R 呈负相关；激光功率与焊接速度的交互作用对 ψ 的影响显著；送丝速度与焊接速度的交互作用对 R 的影响显著。当 $\psi = 1.1 \sim 1.2$，$R = 0.2 \sim 0.3$ 时，最终工艺优化区间为 $P = 4120 \sim 4300$ W，$V_{\mathrm{w}} = 15.3 \sim 16.3$ mm/s，$V_{\mathrm{f}} = 12.3 \sim 13.6$ m/min。

3）选择参数 $P = 4250$ W、$V_{\mathrm{w}} = 16$ mm/s、$V_{\mathrm{f}} = 13$ m/min 与 $P = 4200$ W、$V_{\mathrm{w}} = 15.5$ mm/s、$V_{\mathrm{f}} = 13$ m/min 进行试验验证，获得成形良好的焊缝，ψ 和 R 模型的准确度分别为 95.0%、92.3%。

参 考 文 献

[1] 虞大联, 邓小军, 刘韶庆, 等. 复合材料技术在转向架中的应用[J]. 电力机车与城轨车辆, 2015, 38(S1): 17-22.
Yu D L, Deng X J, Liu S Q, et al. Application of composite material technology on bogie[J]. Electric Locomotives & Mass Transit Vehicles, 2015, 38(S1): 17-22.

[2] 刘婷, 赵艳秋, 周旭东, 等. 能量配比系数对铝合金激光-MIG复合焊接气孔的影响[J]. 中国激光, 2020, 47(11): 1102004.
Liu T, Zhao Y Q, Zhou X D, et al. Effect of energy ratio coefficient on pore during aluminum alloy laser-MIG hybrid welding [J]. Chinese Journal of Lasers, 2020, 47(11): 1102004.

[3] 邓德伟, 吕捷, 马玉山, 等. FV520B 钢激光打底焊结合 CMT填充焊焊接接头的组织和性能[J]. 中国激光, 2020, 47(11): 1102001.
Deng D W, Lü J, Ma Y S, et al. Microstructures and properties of FV520B steel joint by laser backing welding with CMT filler welding[J]. Chinese Journal of Lasers, 2020, 47(11): 1102001.

[4] Hanji T, Tateishi K, Shimizu M, et al. Fatigue strength of cruciform joints and longitudinal joints with laser-arc hybrid welding[J]. Welding in the World, 2019, 63(5): 1379-1390.

[5] Vorontsov A, Zykova A, Chumaevskii A, et al. Advanced high-strength AA5083 welds by high-speed hybrid laser-arc welding[J]. Materials Letters, 2021, 291: 129594.

[6] 雷正龙, 黎炳蔚, 周恒, 等. 端接接头激光-MAG 复合焊熔滴过渡与气孔特征分析[J]. 中国激光, 2019, 46(3): 0302007.
Lei Z L, Li B W, Zhou H, et al. Analysis of droplet transfer and porosity characteristics in laser-MAG hybrid welding of edge joint[J]. Chinese Journal of Lasers, 2019, 46(3): 0302007.

[7] Yang X Y, Chen H, Zhu Z T, et al. Effect of shielding gas flow on welding process of laser-arc hybrid welding and MIG welding [J]. Journal of Manufacturing Processes, 2019, 38: 530-542.

[8] Wang L, Gao M, Hao Z Q. A pathway to mitigate macrosegregation of laser-arc hybrid Al-Si welds through beam oscillation[J]. International Journal of Heat and Mass Transfer, 2020, 151: 119467.

[9] 马彦龙, 陈辉, 赵旭, 等. 1000 MPa 级超高强钢激光复合焊接头力学性能研究[J]. 中国激光, 2021, 48(6): 0602113.
Ma Y L, Chen H, Zhao X, et al. Mechanical properties of laser hybrid welded joint of 1000 MPa ultrahigh-strength steel[J]. Chinese Journal of Lasers, 2021, 48(6): 0602113.

[10] 陈志伟, 马程远, 陈波, 等. 激光-MIG 复合焊接中厚度不锈钢组织及性能研究[J]. 激光与光电子学进展, 2020, 57(23): 231405.
Chen Z W, Ma C Y, Chen B, et al. Microstructure and properties of medium-thick stainless steel by laser-MIG hybrid welding[J]. Laser & Optoelectronics Progress, 2020, 57(23): 231405.

[11] 杜永鹏, 郭宁, 吴程皞, 等. 焊缝余高变异系数在水下湿法焊接质量评估过程中的应用[J]. 焊接学报, 2020, 41(2): 24-27, 32, 98.
Du Y P, Guo N, Wu C H, et al. Study on the application of the weld reinforcement variation coefficient in underwater wet welding quality evaluation [J]. Transactions of the China Welding Institution, 2020, 41(2): 24-27, 32, 98.

［12］ 张正浩, 王传强, 齐恩语, 等. 核级高硅含钛不锈钢激光-电弧复合焊接工艺及接头组织性能［J］. 中国激光, 2021, 48(14): 1402008.
Zhang Z H, Wang C Q, Qi E Y, et al. Laser-arc hybrid welding process and joint microstructure and properties of nuclear grade high silicon titanium-containing stainless steel［J］. Chinese Journal of Lasers, 2021, 48(14): 1402008.

［13］ Liu G Q, Gao X D, Peng C, et al. Optimization of laser welding of DP780 to Al5052 joints for weld width and lap-shear force using response surface methodology［J］. Optics & Laser Technology, 2020, 126: 106072.

［14］ Ji X R, Hua X M, Shen C, et al. Optimization of welding parameters on pores migration in laser-GMAW of 5083 aluminum alloy based on response surface methodology［J］. Applied Sciences, 2019, 1(10): 1-12.

［15］ Vasantharaja P, Vasudevan M. Optimization of A-TIG welding process parameters for RAFM steel using response surface methodology［J］. Proceedings of the Institution of Mechanical Engineers, Part L: Journal of Materials: Design and Applications, 2018, 232(2): 121-136.

［16］ Acherjee B, Misra D, Bose D, et al. Prediction of weld strength and seam width for laser transmission welding of thermoplastic using response surface methodology［J］. Optics & Laser Technology, 2009, 41(8): 956-967.

［17］ Srichok T, Pitakaso R, Sethanan K, et al. Combined response surface method and modified differential evolution for parameter optimization of friction stir welding［J］. Processes, 2020, 8(9): 1080.

［18］ Babu N, Natarajan U, Malayalamurthi R. Evaluating mechanical and metallurgical properties of gas tungsten arc welded AA 5059 aluminium alloy joints［J］. Materials Today: Proceedings, 2020, 22: 353-363.

［19］ Sharma P, Mohal S. Parametric optimization of submerged arc welding process parameters by response surface methodology［J］. Materials Today: Proceedings, 2020, 24: 673-682.

［20］ 陈超, 陈芙蓉, 张慧婧. 响应面法分析 7A52 铝合金光纤激光焊气孔敏感性［J］. 焊接, 2016(5): 17-21, 73.
Chen C, Chen F R, Zhang H J. Porosity sensitivity analysis of 7A52 aluminum alloy during fiber laser welding by response surface method［J］. Welding & Joining, 2016(5): 17-21, 73.

［21］ 褚振涛, 于治水, 张培磊, 等. 基于响应面分析的 T 型接头激光深熔焊焊缝形貌预测及工艺参数优化［J］. 中国激光, 2015, 42(2): 0203006.
Chu Z T, Yu Z S, Zhang P L, et al. Weld profile prediction and process parameters optimization of T-joints of laser full penetration welding via response surface methodology［J］. Chinese Journal of Lasers, 2015, 42(2): 0203006.

［22］ Ragavendran M, Chandrasekhar N, Ravikumar R, et al. Optimization of hybrid laser-TIG welding of 316LN steel using response surface methodology (RSM)［J］. Optics and Lasers in Engineering, 2017, 94: 27-36.

［23］ Reisgen U, Schleser M, Mokrov O, et al. Optimization of laser welding of DP/TRIP steel sheets using statistical approach［J］. Optics & Laser Technology, 2012, 44(1): 255-262.

［24］ Wang X, Zhang C, Wang K, et al. Multi-objective optimization of laser transmission joining of thermoplastics［J］. Optics & Laser Technology, 2012, 44(8): 2393-2402.

［25］ Benyounis K Y, Olabi A G, Hashmi M S J. Effect of laser welding parameters on the heat input and weld-bead profile［J］. Journal of Materials Processing Technology, 2005, 164/165: 978-985.

［26］ 孙硕. 高强钢激光-电弧复合焊焊缝成型的预测研究［D］. 长春: 长春理工大学, 2014.
Sun S. The prediction of weld bead shape for high-strength steel by laser-arc hybrid welding［D］. Changchun: Changchun University of Science and Technology, 2014.

［27］ 孙硕, 刘双宇, 贾冬生, 等. 高氮钢激光-电弧复合焊焊缝成形多元非线性回归模型［J］. 机械工程学报, 2015, 51(8): 67-75.
Sun S, Liu S Y, Jia D S, et al. Multiple nonlinear regression model of weld bead shape for high nitrogen steel by laser-arc hybrid welding［J］. Journal of Mechanical Engineering, 2015, 51(8): 67-75.

Process Parameter Optimization for Laser-Arc Hybrid Welding of Low-Carbon Bainite Steel Based on Response Surface Methodology

Yu Jie, Cai Chuang[*], Xie Jia, Liang Ying, Huang Jiasen, Liu Zhijie, Liu Yonghong

Key Laboratory of Advanced Technologies of Materials, Ministry of Education, School of Materials Science and Engineering, Southwest Jiaotong University, Chengdu 610031, Sichuan, China

Abstract

Objective　Low-carbon bainite steel has the advantages including high toughness and high specific strength, and has become the main material for the manufacture of high-speed train bogies which have increasingly stringent requirements for light-weighting. There are many butt joints and T-joints in bogies, which urgently need the high efficiency and quality welding technologies. Compared with MAG welding (MAG welding, metal active gas arc welding), the laser-arc hybrid welding with the combination of laser with arc improves the welding efficiency and reduces the welding defects. The laser-arc hybrid welding has a greater prospect of application in the welding of low-carbon bainite steel for high-speed train bogies. However, the parameter optimization for laser-arc hybrid welding is costly and time-consuming. The changes in the welding parameters and the interaction among the welding parameters cause the change in the weld formation. The response surface methodology (RSM) is used to study the influence of various parameters and the interaction among parameters on the response indexes, which is beneficial to achieve the parameter optimization for the laser-arc hybrid welding process. However, most studies have focused on the application of the response surface optimization analysis in the optimization of the single heat source welding process. Few studies have focused on the response surface optimization analysis for the hybrid heat sources. Here, the influence of various parameters and the interaction among parameters on

the welding morphology is studied for laser-MAG hybrid welding of 6 mm thick low-carbon bainite steel butt joints based on the response surface methodology. The welding process parameters are optimized and tested. It is verified that the process optimization for laser-MAG hybrid welding of new low-carbon bainite steel is realized.

Methods A new type of low-carbon bainite steel plate with a size of 350 mm × 175 mm × 6 mm is used as the base metal, and the welding wire with a diameter of 1.2 mm is adopted as the filler wire. The 10 kW fiber laser and the arc from welding machine are used as the heat source. A robot and an integrated operation control cabinet are equipped in the welding system. A laser leading mode is adopted for laser-MAG hybrid welding, the I-shaped groove with a butt gap of 1.0 mm is adopted in the experiment, and single-sided formation and double-sided welding formation are obtained. The welding test plate is placed on a horizontal workbench. In order to prevent laser reflection from damaging the internal structure of the laser, the angle of laser beam relative to the vertical direction is set as 10°. The angle of welding torch relative to the test plate is set as 40°. The distance between laser and filler wire is 2 mm. The laser defocused distance is 0 mm during welding. The shielding gas of Ar + CO_2 mixture with a gas flow rate of 25 L/min is used. (Fig. 1). The microscope is used to observe and photograph the morphologies of welded joints. The weld width (W), penetration depth (H), arc zone area (S_1), and laser zone area (S_2) are first measured by the Image-Pro software. Then the weld forming coefficient (ψ) and the laser zone area ratio (R) are calculated to characterize the shape and size of the weld and the proportion of laser energy in the total energy, respectively. The test results are arranged, counted, and analyzed by the Design-Expert software.

Results and Discussions The mathematical models for the weld formation coefficient ψ and the laser area ratio R are established based on the experimental factors and response statistics. According to the F test, the reliabilities of the ψ and R models are excellent. With the increase of laser power (P), ψ first increases and then decreases. With the increase of welding speed (V_w), ψ gradually decreases. With the increase of wire feeding speed (V_f), the formation coefficient ψ increases slowly. As shown in the response surface diagram of ψ versus P and V_w, ψ is high due to the large volume of molten metal, the big weld penetration depth and width caused by the low laser power and welding speed. $\psi = 1.1$–1.2 is first determined by the experimental parameters of joints with well formation, and then the optimized parameter interval $P = 4000$–4300 W and $V_w = 15.1$–16.3 mm/s are obtained. The response surface diagram of ψ versus P and V_f illustrates that the optimized parameter range is $P = 3970$–4370 W and $V_f = 10.9 - 14.5$ m/min. The response surface diagram of ψ versus V_w and V_f indicates that V_w has a significant impact on ψ, while V_f has a relatively small impact on ψ. The optimization interval is $V_w = 15.3$–16.6 mm/s and $V_f = 12.3$–13.6 m/min (Fig. 3). In the R model, R first increases and then decreases with the increase of P and V_w. R has a gradual upward trend with the increase of V_f. The response surface diagram of R versus P and V_w illustrates that R is high when the welding speed is low. According to the 6th and 16th tests, $R = 0.2$–0.3 is determined, and the corresponding optimization interval is $P = 4120$–4300 W and $V_w = 14.8$–16.4 mm/s. The response surface diagram of R versus P and V_f shows that both P and V_f have little impact on R, and the optimization interval is $P = 4100$–4320 W and $V_f = 10.6$–13.9 m/min. According to the response surface diagram of R versus V_w and V_f, the optimization interval is $V_w = 13.9$–16.4 mm/s and $V_f = 11.5$–13.6 m/min (Fig. 4). Based on the above analysis, the final optimization interval is $P = 4120$–4300 W, $V_w = 15.3$–16.3 mm/s, and $V_f = 12.3$–13.6 m/min. $P = 4250$ W, $V_w = 16$ mm/s, $V_f = 13$ m/min, and $P = 4200$ W, $V_w = 15.5$ mm/s, and $V_f = 13$ m/min are selected for test verification, respectively. The obtained weld is well formed and the accuracies of ψ and R models are 95.0% and 92.3%, respectively.

Conclusions Based on the response surface methodology, two statistical models of the appearance quality of the low-carbon bainite steel welded joints by laser-MAG hybrid welding under different laser powers, welding speeds, and wire feeding speeds are established. In the models, wire feeding speed has a significant influence on ψ and P. Welding speed is negatively relative to ψ and P. The interaction between laser power and welding speed has a significant influence on ψ. The interaction between wire feeding speed and welding speed has a significant influence on R. When $\psi = 1.1$–1.2 and $R = 0.2$–0.3, the process parameters of laser power, welding speed, and wire feeding speed are optimized as $P = 4120$–4300 W, $V_w = 15$–16 mm/s, and $V_f = 12$–14 m/min. The parameters of $P = 4250$ W, $V_w = 16$ mm/s, $V_f = 13$ m/min, and $P = 4200$ W, $V_w = 15.5$ mm/s, and $V_f = 13$ m/min are selected for the experimental verification, respectively. The obtained weld is well formed. The accuracies of the ψ and R models are 95.0% and 92.3%, respectively.

Key words laser technique; laser-MAG hybrid welding; low carbon bainite steel; response surface methodology; forming coefficient; laser area ratio